IOP Publishing Nanotechnology
Nanotechnology 28 (2017) 105703 (6pp) https://doi.org/10.1088/1361-6528/aa5962

Nanoscale mapping of optical band gaps using monochromated electron energy loss spectroscopy

W Zhan[1], C S Granerød[1], V Venkatachalapathy[1], K M H Johansen[1], I J T Jensen[2], A Yu Kuznetsov[1] and Ø Prytz[1]

[1] Department of Physics, Centre for Materials Science and Nanotechnology, University of Oslo, PO Box 1048—Blindern, NO-0316 Oslo, Norway
[2] SINTEF Materials and Chemistry, PO Box 124—Blindern, NO-0314 Oslo, Norway

E-mail: oystein.prytz@fys.uio.no

Received 17 October 2016, revised 18 December 2016
Accepted for publication 13 January 2017
Published 3 February 2017

Abstract

Using monochromated electron energy loss spectroscopy in a probe-corrected scanning transmission electron microscope we demonstrate band gap mapping in ZnO/ZnCdO thin films with a spatial resolution below 10 nm and spectral precision of 20 meV.

Keywords: electron energy loss spectroscopy, STEM, ZnO, band gap engineering

(Some figures may appear in colour only in the online journal)

1. Introduction

Tailoring material properties by controlling nanometer scale structure and composition is of increasing importance in many fields of modern physics and nanoscience. The key issue here is the ability to observe and measure the materials' properties at the corresponding length scales. In this respect, modern transmission electron microscopy (TEM) is an essential tool, allowing structural and chemical information to be obtained at sub-ångström scales. In addition to its unrivaled spatial resolution for imaging and diffraction, modern TEM also provides a wealth of analytical signals that can be used for materials analysis. In fact, one can consider the electron beam simply as a broad-band source of electromagnetic radiation, and the TEM can be viewed as an in-house beam line that allows us to perform many experiments normally undertaken by using photons, but now with orders of magnitude better spatial resolution.

The recent decade's technical developments of Cs correctors and electron beam monochromators have started bearing out this promise [1–11], giving the materials research community access to new ways of studying devices and structures at the nanoscale. In particular, analytical signals observed using electron energy loss spectroscopy (EELS) are of great interest. Here we monitor the energy loss of a monochromatic electron beam due to excitation processes in the sample. Taking advantage of the high spatial resolution of the electron beam, mapping of the local geometries of systems and their optical response through surface plasmon polaritons and localized surface plasmons [12–14], and band gap excitations can be performed [15–19].

In the simplest case of single electron excitations, the energy loss intensity is related to the double differential cross section [15, 20, 21]:

$$\frac{\mathrm{d}^2\sigma(E,\mathbf{q})}{\mathrm{d}E\ \mathrm{d}\mathbf{q}} = \frac{4\gamma^2}{a_0^2\mathbf{q}^4}\rho(E)\left|\langle\Psi_f|\mathrm{e}^{\mathrm{i}\mathbf{q}\cdot\mathbf{r}}|\Psi_i\rangle\right|^2. \quad (1)$$

Here the process is described as an electron in the initial state $|\Psi_i\rangle$ that is excited into an empty state $|\Psi_f\rangle$ above the Fermi-level by absorbing energy from the incident electron. E is the difference in the energy of the final and initial states, and $\mathbf{q}$ is the momentum transfer. γ is the relativistic correction factor, a_0 is the first Bohr radius, and $\rho(E)$ is the joint density of states resulting from the convolution of the density of initial and final states. $\mathbf{r}$ is the coordinate of the fast electron. When investigating the band gaps of semiconductors, the initial and final states are the valence and conduction bands respectively, and the minimum energy transfer corresponds to the band gap energy.

In the approximation of direct transitions between two parabolic bands, it has been shown [20] that the energy loss intensity close to the band gap absorption energy is expected to have the simple form

$$I(E) = c\sqrt{E - E_g}, \quad (2)$$

where c is a scaling factor, E is the energy loss, and E_g is the band gap energy. Thus, the observed EELS intensity can closely match what is observed in optical experiments, thereby allowing us to extract the optical band gap from EELS spectra with sufficient energy resolution and statistical quality [15–19].

However, even though modern TEM instruments now routinely achieve electron beams of sub-ångström size, the spatial resolution of the EELS experiment may not necessarily be comparable. For low energy transitions the incident fast electron can transfer sufficient energy over much longer distances. Previous studies have shown that such inelastic delocalization may obscure the local information, thereby limiting the effective resolution obtained in the low loss EELS experiment [22–24]. Lin Gu and co-workers estimated the delocalization to be about 12 nm for energy losses around 3 eV [16], similar to Bosman *et al* who concluded that the spatial resolution limits for transistions in the same energy range is around 10 nm [18]. In both cases, the experimental estimates are significantly higher than theoretical estimates that indicate an inelastic delocalization (L_{50}) of 3–7 nm for band gap transitions in common semiconductors [25].

In this study we experimentally address the limits of the spatial resolution and spectral precision in monochromated EELS band gap measurements using the wide band gap semiconductor ZnO ($E_g \approx 3.3$ eV) alloyed with CdO as a model system. We show that in such systems, the band gap can be mapped with a spectral precision of 20 meV and a spatial resolution below 10 nm.

2. Experimental setup and data analysis

The measurements were performed on a $ZnO/Zn_{1-x}Cd_xO$ thin film structure grown by metal organic vapor phase epitaxy on c-oriented α-Al_2O_3 substrate. The samples consist of two layers, first approximately 120 nm of pure ZnO buffer layer, followed by 120 nm of ZnO alloyed with CdO. The samples were investigated using x-ray diffraction, and were found to be single phase wurtzite with no indication of rs-CdO. The band gap of the alloy can be tuned as a function of the Zn/Cd ratio [26–28], e.g. for compositions $Zn_{1-x}Cd_xO$, $x = 0$–0.67 the band gap was found to vary between 3.25 and 1.7 eV [29].

Samples for scanning transmission electron microscopy (STEM) were prepared by standard cross sectional sample preparation techniques, giving TEM specimens of approximately 20–30 nm thickness. The samples were plasma cleaned using a Fischione Model 1020 plasma cleaner directly before the STEM experiments in order to avoid carbon contamination. The STEM investigations were performed in a probe-corrected and monochromated FEI Titan G2 60–300 equipped with the FEI Super-X EDX detectors. An accelerating voltage of 300 kV was used for the structural and chemical characterization. At such high acceleration voltage, the speed of the electrons may exceed the speed of light in the material producing Cherenkov radiation in the visible spectrum, which will interfere with the EELS spectrum. Therefore, an accelerating voltage of 60 kV was used to obtain the EELS spectra, thereby reducing the probability of generating Cherenkov radiation. Following the work of Erni and Browning (equation (6) in [30]), the normalized probability per unit path length (P^*) was assessed to be on the order of 0.2, which combined with the relatively thin sample (<30 nm) leads us to expect no significant contribution to the energy loss spectrum from Cherenkov photons at the current experimental conditions.

The EELS measurements were performed in probe-corrected STEM mode with an energy resolution of approximately 0.15 eV as measured by the full-width at half maximum of the zero loss peak (ZLP). The data were acquired in the form of spectrum images, where the beam was scanned in two spatial dimensions with an energy-loss spectrum associated with each pixel. Since the band gap energy is given by the onset of energy loss, direct mapping methods often used in the field of EELS-plasmonics involving selecting an energy window and mapping the spatial distribution of intensities are not suitable to create band gap maps. In this work we instead extract the band gap at each position of the beam through a combination of fitting and subtracting the background, followed by fitting of the energy loss model (equation (2)) to the experimental data.

The first step is to align the individual spectra to the maximum of the ZLP, before removing the background originating from the tail of the ZLP by fitting an exponentially falling intensity. As suggested in [30, 31], this approach to background subtraction may be suitable for wide band gap materials with insignificant surface or retardation losses. In this case it was found to give more robust and reproducible results than subtracting a pre-measured ZLP in vacuum. However, the exact fit range of the background model influences the extracted band gap value, as will be discussed in the following section.

To enhance the signal to noise ratio, a 2×2 binning of the original data was performed. Furthermore, Sawitsky–Golay smoothing filters were also applied. The band gap value in each pixel was then extracted by a curve fitting method based on the approach proposed by Rafferty and Brown [20]. A visual identification of an energy loss range which includes the onset and increasing intensity of energy loss gives a fit range up to 3.5 eV. All energy points in this range are used as test values and checked iteratively by fitting equation (2) using the test value as the onset energy E_g. The only fit parameter is then the scaling factor c, and the band gap is determined as the test value giving the highest goodness-of-fit as judged from the the correlation factor R^2.

The band gap values as observed in the EELS experiments were compared with that measured by cathode luminescence (CL) using a DELMIC SPARC detector mounted in a Hitatchi SU5000 operated with a 7 kV electron beam. Under these conditions, the electrons have enough energy to

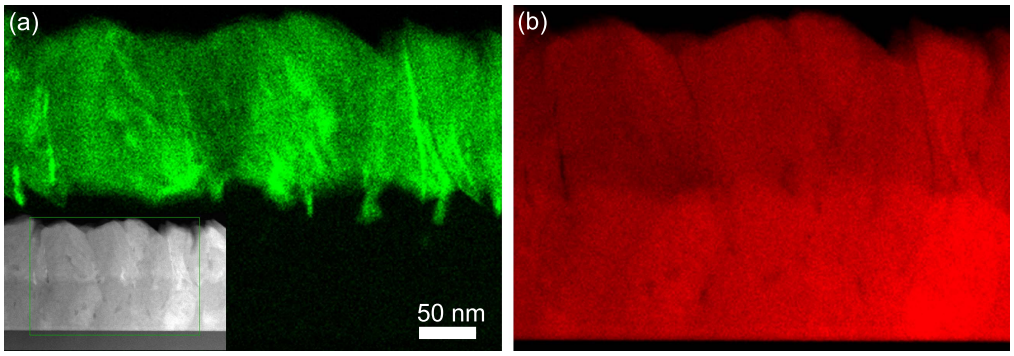

Figure 1. STEM-EDX mapping of the Cd (a) and Zn (b) concentrations. The inset in (a) shows a high-angle annular dark-field STEM image displaying atomic number contrast in the sample.

penetrate through the Cd-containing layer into the ZnO buffer layer.

3. Results and discussion

Figure 1 shows a compositional map acquired by energy dispersive x-ray spectroscopy (EDX). The mapping shows that the interface between the layers is not entirely sharp, with lateral roughness at the 50 nm scale. In addition to this large scale interface roughness, we observe smaller tendrils of Cd rich material penetrating into the ZnO layer. These tendrils are some tens of nanometers long, and between 5 and 10 nm in cross section. Furthermore, the Cd-containing film displays significant internal chemical inhomogeneity. The observed compositional range is roughly $x = 0.1$–0.2, with higher and lower concentrations appearing in localized regions. Altogether these features provide a good case for investigating the frontiers of spatial resolution and spectral precision in EELS band gap measurements.

EELS spectrum images and EDX compositional maps were obtained from the same region of the sample, and band gaps were extracted according to the procedure described previously. The resulting band gap values depend on the choice of the fitting region for the background subtraction. For the most accurate results, this fitting region should be chosen close to the expected onset of the band gap transitions being studied. Choosing the fitting region at 2.4–2.9 eV and extracting the band gap from 204 pixels in a chemically homogeneous region of the ZnO buffer layer results in an average band gap of $\overline{E_g} = 3.22$ eV with standard deviation $\sigma = 0.02$ eV as shown in figure 2. These values are representative of similar measurements performed on several separately prepared samples, and are in good agreement with the value 3.23 eV obtained in this study using CL-measurements (see the inset in figure 2) and observations of the absorption using UV–vis photospectrometry (not shown). This shows that both excellent accuracy and precision can be obtained using EELS band gap measurements.

The observed values of the band gap are, however, somewhat lower than the usually quoted values for bulk ZnO (≈3.3 eV). To understand this it is important to realize that similar to optical absorption measurements the energy loss

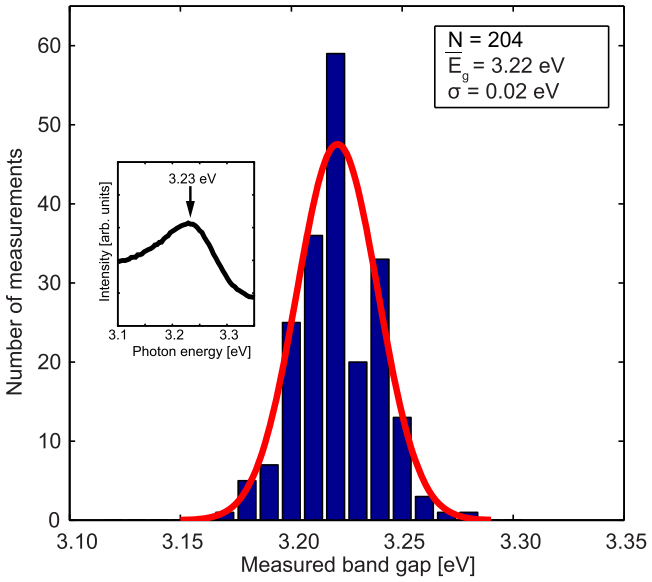

Figure 2. Histogram of the band gap values as extracted from the pure ZnO buffer layer. A Gaussian fitting is superimposed. The small spread of values indicates a high precision in the measured values. The inset shows the CL spectrum displaying emission associated with the band gap at approximately 3.23 eV.

experiments measure the onset of absorption, also referred to as the optical band gap. In ZnO, the large exciton binding energy reduces the optical gap significantly compared to the fundamental gap. Furthermore, the optical gap is influenced by the crystalline quality, grain size, defects, and strain, often reducing the gap even further [32–36]. Bundesmann and coworkers compiled a summary of values measured with different techniques on thin film specimens with varying quality and under different growth conditions [37]. The observed optical gap in this compilation varies between 3.195 and 3.44 eV, with most values clustering around 3.24–3.28 eV. We therefore conclude that the observed values are in good agreement with literature.

When creating band gap maps over a larger, chemically inhomogeneous region, the choice of background fitting range becomes more challenging. With the cadmium concentration locally reaching high values of $x = 0.25$, we must anticipate that the band gap may shift well into the fitting range chosen for the pure ZnO. A lower fitting range must therefore be

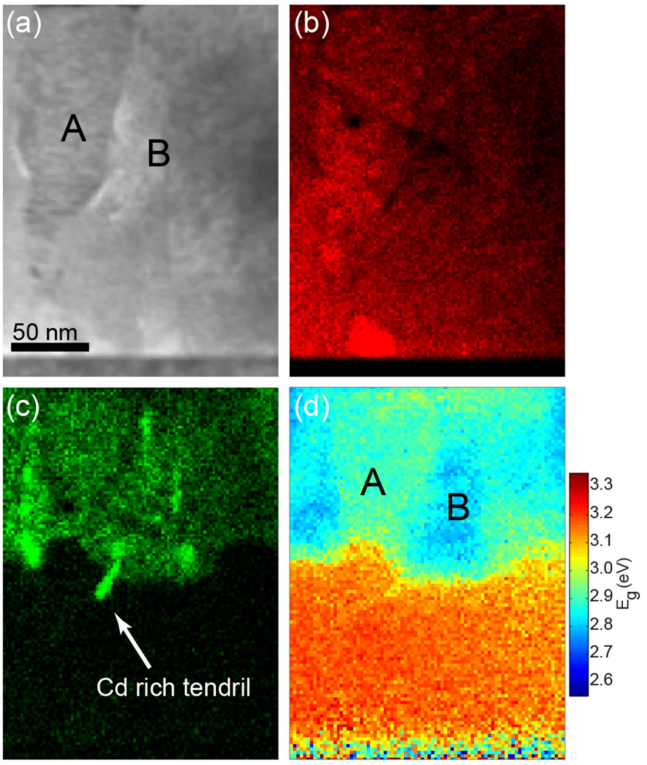

Figure 3. (a) ADF-STEM image showing chemical and structural variations in the sample. (b) Zn EDX map (c) Cd EDX map, and (d) corresponding map of the extracted band gaps.

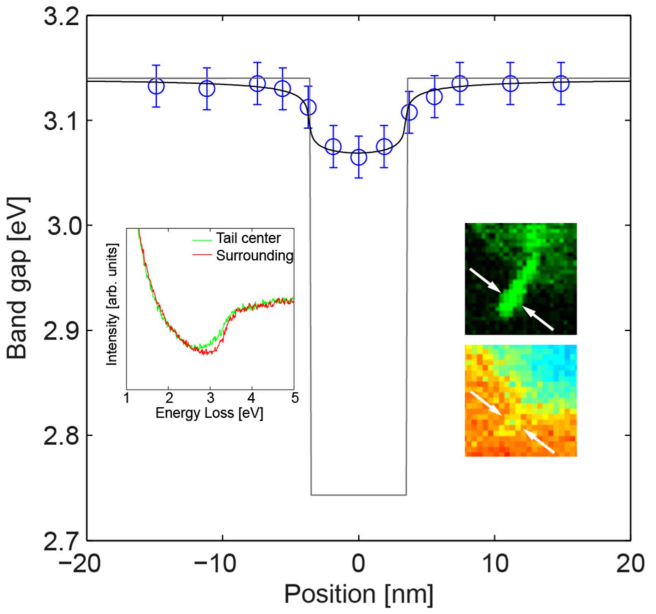

Figure 4. Experimentally observed variation of the extracted band gap across the Cd rich tendril in figure 3 (open circles), compared with the square well model (gray), and the simulated line profile (black). See the text for more details. The inset on the left shows the EELS spectra from the center of the tendril (green) and surrounding matrix (red). The insets on the right are closeups of the Cd and band gap maps in figures 3(c) and (d) respectively.

chosen to ensure success in the band gap extraction over the whole compositional range, although this will reduce the accuracy for the pure ZnO layer. Testing different fitting ranges shows that a systematic downward shift of 20–40 meV must be expected for the extracted band gap of the ZnO layer. However, the precision is not affected, meaning that the very high sensitivity to variations in the band gap is retained. Specifically, the band gap map resulting from a background fitting region of 1.75–2.25 eV is shown in figure 3(d) together with an annular dark-field STEM image and EDX mapping from Zn Kα and Cd Lα characteristic x-ray peaks.

Turning now to the spatial variations of the band gap, we can conclude that we have sufficient sensitivity to detect the band gap changes due to quite small compositional variations. For example, a band gap difference of 0.11 eV between the Cd poor grain marked *A* in figure 3(a) ($x = 0.07$) and the adjacent area *B* ($x = 0.14$) is readily resolved. Furthermore, along the interface between the pure ZnO and the Cd containing films, the band gap map closely matches the observed chemical interface roughness. In particular we note that the tendril of Cd rich material penetrating into the ZnO layer seen in the EDX mapping is also observed in the band gap map. This feature is approximately 19 nm long and 7.5 nm wide in cross section, with an average Cd concentration of $x \approx 0.23$. This Cd concentration is at the higher end of what is observed anywhere in the Cd-containing part of the film. We therefore do not expect there to be significant amounts of ZnO above or below the tendril along the beam path, as the opposite case would imply an implausibly high Cd concentration in the tendril. Thus, we assume that the tendril extends through the entire thickness of the sample, making it a prime opportunity to evaluate the attainable spatial resolution of the EELS band gap method.

In figure 4 we have plotted the extracted band gap across the tail, and a statistically significant drop of $\approx 3.5\sigma$ is observed between the center of the tendril and the adjacent areas, with a minimum observed band gap of 3.07 eV in the center of the tendril. However, when using the band bowing parameters reported by Wang and co-workers [27] we find that this observed minimum of the band gap is higher than expected from the observed Cd concentration. Indeed, a composition of $x \approx 0.23$ should give $E_g \approx 2.77$ eV.

This discrepancy between the observed band gap and the expected value can be explained by the electron beam interacting both locally in the ZnCdO tendril and with the adjacent ZnO, thereby giving an energy loss spectrum which might be interpreted as a higher E_g by the fitting procedure. While this delocalized interaction of the electron beam is unavoidable and limits the attainable spatial resolution, our results indicate that a spatial resolution better than 10 nm can be achieved. To investigate if the actual band gap profile can be reconstructed from experimental data, we simulate the observed band gap profile as a convolution of the actual profile with a spatial point spread function (PSF) which describes the effect of delocalized interaction.

As input to this analysis, we need a quantitative description of the PSF, which can be obtained through a full analysis of the scattering mechanisms [25]. However, we note that the PSF resembles the potential surrounding a point charge $V(r) \propto 1/r$ [25, 38]. Thus, by scaling it to the to the

delocalization length $L_{50} = 5.8$ nm, which includes 50% of the inelastic interactions, a simple model for the PSF is proposed. Such a scaling is consistent with what should be expected for energy losses around 3 eV [21, 25], and means that for each point in the spectrum image, 50% of the observed signal originates inside a diameter of 5.8 nm, while 50% originates outside.

The PSF described above is convoluted with a model for the actual band gap profile. In accordance with the discussion previously, we assume that the tendril extends through the whole thickness of the film, and that the interface is sharp. The band gap profile then resembles a square well, with a high band gap outside the tendril and lower band gap inside it. We then iteratively simulate the observed profile as the convolution of the PSF with this model profile, using the width and depth of the square well model as fitting parameters until a best fit to the observed data is found. The resulting square well model and simulated profile are shown in figure 4 together with the experimentally observed band gap values.

Given the assumptions made above, a perfect match with the experimental data is not expected. Nevertheless, the best fit was found for a square well 6.85 nm in width, with a minimum band gap value of 2.74 eV corresponding to $x \approx 0.24$. Although these values deviate somewhat from our observations (7.5 nm and $x \approx 0.23$ with expected band gap of 2.77 eV), the similarities are striking. We therefore conclude that spatial resolution well below 10 nm can be achieved in EELS band gap measurements, and that the absolute value of the band gap can be retrieved from the experimental data by employing relatively simple modeling.

4. Conclusions

In this work we have shown that spatial resolution well below 10 nm can be achieved with unprecedented precision in monochromated EELS band gap measurements. This is close to what can be considered as a theoretical limit for the spatial resolution of electron energy loss band gap mapping. Thus, EELS provides an excellent tool for investigations of local band gap gradients on the scale of a few nanometers, and may significantly aid in improving the quality of interface control in the field of band gap engineering of semiconductors.

Acknowledgments

The Research Council of Norway is acknowledged for the support to the Norwegian Center for Transmission Electron Microscopy, NORTEM (197405/F50) and the Norwegian Micro- and Nano-Fabrication Facility, NorFab (197411/V30). K M Johansen would also like to thank the Research Council of Norway for the support through the DYNAZOx project (no. 221992).

References

[1] Batson P E, Dellby N and Krivanek O L 2002 Sub-ångstrom resolution using aberration corrected electron optics *Nature* **418** 617–20

[2] Tizei L H G, Lin Y-C, Mukai M, Sawada H, Lu A-Y, Li L-J, Kimoto K and Suenaga K 2015 Exciton mapping at subwavelength scales in two-dimensional materials *Phys. Rev. Lett.* **114** 107601

[3] Urban A, Müller M, Karbaum C, Schmidt G, Veit P, Malindretos J, Bertram F, Christen J and Rizzi A 2015 Optical emission of individual GaN nanocolumns analyzed with high spatial resolution *Nano Lett.* **15** 5105–9

[4] Tan H, Turner S, Yücelen E, Verbeeck J and Van Tendeloo G 2011 2D atomic mapping of oxidation states in transition metal oxides by scanning transmission electron microscopy and electron energy-loss spectroscopy *Phys. Rev. Lett.* **107** 107602

[5] Cantoni C *et al* 2012 Electron transfer and ionic displacements at the origin of the 2D electron gas at the LAO/STO interface: direct measurements with atomic-column spatial resolution *Adv. Mater.* **24** 3952–7

[6] Erni R, Rossell M D, Kisielowski C and Dahmen U 2009 Atomic-resolution imaging with a sub-50 pm electron probe *Phys. Rev. Lett.* **102** 096101

[7] Horton M K, Rhode S, Sahonta S-L, Kappers M J, Haigh S J, Pennycook T J, Humphreys C J, Dusane R O and Moram M A 2015 Segregation of In to dislocations in InGaN *Nano Lett.* **15** 923–30

[8] Wei J, Jiang N, Xu J, Bai X and Liu J 2015 Strong coupling between ZnO excitons and localized surface plasmons of silver nanoparticles studied by STEM-EELS *Nano Lett.* **15** 5926–31

[9] Ishikawa R, Lupini A R, Findlay S D, Taniguchi T and Pennycook S J 2014 Three-dimensional location of a single dopant with atomic precision by aberration-corrected scanning transmission electron microscopy *Nano Lett.* **14** 1903–8

[10] Losquin A *et al* 2015 Unveiling nanometer scale extinction and scattering phenomena through combined electron energy loss spectroscopy and cathodoluminescence measurements *Nano Lett.* **15** 1229–37

[11] Kothleitner G, Neish M J, Lugg N R, Findlay S D, Grogger W, Hofer F and Allen L J 2014 Quantitative elemental mapping at atomic resolution using x-ray spectroscopy *Phys. Rev. Lett.* **112** 085501

[12] Nelayah J, Kociak M, Stephan O, Garcia de Abajo F J, Tence M, Henrard L, Taverna D, Pastoriza-Santos I, Liz-Marzan L M and Colliex C 2007 Mapping surface plasmons on a single metallic nanoparticle *Nat. Phys.* **3** 348–53

[13] Schubert I, Sigle W, van Aken P A, Trautmann C and Toimil-Molares M E 2015 STEM-EELS analysis of multipole surface plasmon modes in symmetry-broken AuAg nanowire dimers *Nanoscale* **7** 4935–41

[14] Cherqui C, Thakkar N, Li G, Camden J P and Masiello D J 2016 Characterizing localized surface plasmons using electron energy-loss spectroscopy *Annu. Rev. Phys. Chem.* **67** 331–57

[15] Gu L, Srot V, Sigle W, Koch C, van Aken P, Scholz F, Thapa S B, Kirchner C, Jetter M and Rühle M 2007 Band-gap measurements of direct and indirect semiconductors using monochromated electrons *Phys. Rev. B* **75** 195214

[16] Gu L, Sigle W, Koch C T, Nelayah J, Srot V and van Aken P A 2009 Mapping of valence energy losses via energy-filtered annular dark-field scanning transmission electron microscopy *Ultramicroscopy* **109** 1164–70

[17] Keller D, Buecheler S, Reinhard P, Pianezzi F, Pohl D, Surrey A, Rellinghaus B, Erni R and Tiwari A N 2014 Local band gap measurements by VEELS of thin film solar cells *Microsc.Microanal.* **20** 1246–53
[18] Bosman M, Tang L J, Ye J D, Tan S T, Zhang Y and Keast V J 2009 Nanoscale band gap spectroscopy on ZnO and GaN-based compounds with a monochromated electron microscope *Appl. Phys. Lett.* **95** 101110
[19] Ye J, Lim S T, Bosman M, Gu S, Zheng Y, Tan H H, Jagadish C, Sun X and Teo K L 2012 Spin-polarized wide electron slabs in functionally graded polar oxide heterostructures *Sci. Rep.* **2** 533
[20] Rafferty B and Brown L M 1998 Direct and indirect transitions in the region of the band gap using electron-energy-loss spectroscopy *Phys. Rev.* B **58** 10326–37
[21] Egerton R F 2011 *Electron Energy-Loss Spectroscopy in the Electron Microscope* 3rd edn (New York: Springer)
[22] Muller D A and Silcox J 1995 Delocalization in inelastic scattering *Ultramicroscopy* **59** 195–213
[23] van Benthem K, French R H, Sigle W, Elsässer C and Rühle M 2001 Valence electron energy loss study of Fe-doped $SrTiO_3$ and a $\Sigma 13$ boundary: electronic structure and dispersion forces *Ultramicroscopy* **86** 303–18
[24] Mory C, Kohl H, Tence M and Colliex C 1991 Experimental investigation of the ultimate EELS spatial resolution *Ultramicroscopy* **37** 191–201
[25] Egerton R F 2007 Limits to the spatial, energy and momentum resolution of electron energy-loss spectroscopy *Ultramicroscopy* **107** 575–86
[26] Venkatachalapathy V, Galeckas A, Trunk M, Zhang T, Azarov A and Kuznetsov A Yu 2011 Understanding phase separation in ZnCdO by a combination of structural and optical analysis *Phys. Rev.* B **83** 125315
[27] Wang X J, Buyanova I A, Chen W M, Izadifard M, Rawal S, Norton D P, Pearton S J, Osinsky A, Dong J W and Dabiran A 2006 Band gap properties of $Zn_{1-x}Cd_xO$ alloys grown by molecular-beam epitaxy *Appl. Phys. Lett.* **89** 151909
[28] Zhu Y Z, Chen G D, Ye H, Walsh A, Moon C Y and Wei S-H 2008 Electronic structure and phase stability of MgO, ZnO, CdO, and related ternary alloys *Phys. Rev.* B **77** 245209
[29] Detert D M, Lim S H M, Tom K, Luce A V, Anders A, Dubon O D, Yu K M and Walukiewicz W 2013 Crystal structure and properties of $Cd_xZn_{1-x}O$ alloys across the full composition range *Appl. Phys. Lett.* **102** 232103
[30] Erni R and Browning N D 2008 The impact of surface and retardation losses on valence electron energy-loss spectroscopy *Ultramicroscopy* **108** 84–99
[31] Stöger-Pollach M 2008 Optical properties and bandgaps from low loss EELS: Pitfalls and solutions *Micron* **39** 1092–110
[32] Minemoto T, Negami T, Nishiwaki S, Takakura H and Hamakawa Y 2000 Preparation of $Zn_{1-x}Mg_xO$ films by radio frequency magnetron sputtering *Thin Solid Films* **372** 173–6
[33] Shan F K and Yu Y S 2003 Optical properties of pure and Al doped ZnO thin films fabricated with plasma produced by excimer laser *Thin Solid Films* **435** 174–8
[34] Srikant V and Clarke D R 1997 Optical absorption edge of ZnO thin films: the effect of substrate *J. Appl. Phys.* **81** 6357–64
[35] Studenikin S A, Golego N and Cocivera M 1998 Optical and electrical properties of undoped ZnO films grown by spray pyrolysis of zinc nitrate solution *J. Appl. Phys.* **83** 2104–11
[36] Zhao J L, Li X M, Bian J M, Yu W D and Gao X D 2005 Structural, optical and electrical properties of ZnO films grown by pulsed laser deposition (PLD) *J. Cryst. Growth* **276** 507–12
[37] Bundesmann C, Schmidt-Grund R and Schubert M 2008 Optical properties of ZnO and related compounds *Transparent Conductive Zinc Oxide* ed K Ellmer *et al* (Berlin: Springer) ch 3 pp 79–124
[38] Garcia de Abajo F J 2010 Optical excitations in electron microscopy *Rev. Mod. Phys.* **82** 209–75